Available online at www.sciencedirect.com
ScienceDirect
Geochimica et Cosmochimica Acta 74 (2010) 5039–5053
Geochimica et Cosmochimica Acta
www.elsevier.com/locate/gca

Constraining magnesium cycling in marine sediments using magnesium isotopes

J.A. Higgins *, D.P. Schrag

Department of Earth and Planetary Science, Harvard University, 20 Oxford St., Cambridge, MA 02138, USA

Received 22 April 2009; accepted in revised form 14 May 2010; available online 25 May 2010

Abstract

Magnesium concentrations in deep-sea sediment pore-fluids typically decrease down core due to net precipitation of dolomite or clay minerals in the sediments or underlying crust. To better characterize and differentiate these processes, we have measured magnesium isotopes in pore-fluids and sediment samples from Ocean Drilling Program sites (1082, 1086, 1012, 984, 1219, and 925) that span a range of oceanographic settings. At all sites, magnesium concentrations decrease with depth. At sites where diagenetic reactions are dominated by the respiration of organic carbon, pore-fluid δ^{26}Mg values increase with depth by as much as 2‰. Because carbonates preferentially incorporate ^{24}Mg (low δ^{26}Mg), the increase in pore-fluid δ^{26}Mg values at these sites is consistent with the removal of magnesium in Mg-carbonate (dolomite). In contrast, at sites where the respiration of organic carbon is not important and/or weatherable minerals are abundant, pore-fluid δ^{26}Mg values decrease with depth by up to 2‰. The decline in pore-fluid δ^{26}Mg at these sites is consistent with a magnesium sink that is isotopically enriched relative to the pore-fluid. The identity of this enriched magnesium sink is likely clay minerals. Using a simple 1D diffusion–advection–reaction model of pore-fluid magnesium, we estimate rates of net magnesium uptake/removal and associated net magnesium isotope fractionation factors for sources and sinks at all sites. Independent estimates of magnesium isotope fractionation during dolomite precipitation from measured δ^{26}Mg values of dolomite samples from sites 1082 and 1012 are very similar to modeled net fractionation factors at these sites, suggesting that local exchange of magnesium between sediment and pore-fluid at these sites can be neglected. Our results indicate that the magnesium incorporated in dolomite is 2.0–2.7‰ depleted in δ^{26}Mg relative to the precipitating fluid. Assuming local exchange of magnesium is minor at the rest of the studied sites, our results suggest that magnesium incorporated into clay minerals is enriched in δ^{26}Mg by 0‰ to +1.25‰ relative to the precipitating fluid. This work demonstrates the utility of magnesium isotopes as a tracer for magnesium sources/sinks in low-temperature aqueous systems.

1. INTRODUCTION

The chemical composition of pore-fluids in marine sediments records interactions between seawater, sediments, and the oceanic crust. Because the concentrations of most elements in the pore-fluid are much lower than their concentrations in the surrounding sediment, reactions in the sediment column and/or underlying basalt often lead to large changes in pore-fluid chemistry but will have little impact on the chemical composition of the solid phases. As a result, the elemental and isotopic composition of sedimentary pore-fluids can be used to study both the distribution and identity of precipitating/dissolving minerals in the sediment column and underlying basalt, even when there are no measurable changes in bulk sediment composition. Extensive sampling of sedimentary pore-fluids by the Deep Sea Drilling Project (DSDP) and Ocean Drilling Program (ODP) has revealed large gradients in major seawater cations (Ca^{2+}, Mg^{2+}) in pore-fluids associated with a range of sediment types (carbonate and siliciclastic) and accumulation rates (Gieskes, 1975; Sayles and Manheim, 1975; Baker, 1985). Although there is some variability, in general,

* Corresponding author. Tel.: +1 617 852 9931.
E-mail address: higgins.ja@gmail.com (J.A. Higgins).

0016-7037/$ - see front matter © 2010 Elsevier Ltd. All rights reserved.
doi:10.1016/j.gca.2010.05.019

the concentration of magnesium in pore-fluid decreases with depth, whereas the concentration of calcium increases. At many sites, magnesium and calcium profiles are approximately linear and associated with decreasing pore-fluid $\delta^{18}O$ values, consistent with low-temperature alteration of the underlying oceanic crust (e.g., Lawrence et al., 1975). However, more complicated profiles are also frequently observed, which has been interpreted as representing significant precipitation and dissolution of carbonate and silicate minerals within the sediment column (Gieskes and Lawrence, 1981; Baker, 1985; Moore et al., 2004), changes in the chemical composition of seawater over time (Fantle and DePaolo, 2006) and/or significant pore-fluid advection (McDuff and Gieskes, 1976).

Measurements of pore-fluid magnesium isotope ratios ($^{25}Mg/^{24}Mg$ and $^{26}Mg/^{24}Mg$) are a potentially useful tool for unraveling the processes responsible for magnesium gradients in deep-sea sediments. Recent work on the variability of magnesium isotope ratios in carbonate and silicate minerals suggests that carbonate minerals are depleted in ^{25}Mg and ^{26}Mg, whereas silicate minerals preferentially retain ^{25}Mg and ^{26}Mg (Galy et al., 2002; Young and Galy, 2004; Tipper et al., 2006b), though there are still uncertainties (Pogge von Strandmann et al., 2008). Galy et al. (2002) and Carder et al. (2005) report magnesium isotope fractionation factors ($\varepsilon_{s-f}^{26/24}$; where $\varepsilon_{s-f}^{26/24} = 1000 \times (\alpha)_{s-f}^{26/24} - 1$ and $(\alpha_{s-f}^{26/24} = (^{26}Mg/^{24}Mg)_s \cdot (^{24}Mg/^{26}Mg)_f)$ for the precipitation of speleothem calcite and dolomite of $-2.7‰$ and $-1.4‰$, respectively, whereas even larger fractionation factors ($\varepsilon_{s-f}^{26/24} \sim -3.5$ to $-4.5‰$) have been observed in foraminiferal calcite (Chang et al., 2004; Pogge von Strandmann, 2008). Estimates of magnesium isotope fractionation during the precipitation of silicate minerals are primarily from measured soil samples and shales, both of which are enriched in $^{26}Mg/^{24}Mg$ ($\varepsilon_{s-f}^{26/24} \sim +0.3$ to $+0.5‰$) compared to primary silicate rocks (Tipper et al., 2006a; Teng et al., 2007). As a result, cycling of magnesium in sedimentary pore-fluids may be expected to produce different profiles in magnesium isotopes depending on whether or not the primary magnesium sources and sinks are carbonate or silicate minerals. In addition to identifying magnesium sources and sinks, pore-fluid profiles of magnesium isotopes can also be used to estimate magnesium isotopic fractionation associated with the precipitation of Mg-minerals, in particular dolomite ($Ca_{0.5}Mg_{0.5}CO_3$) and Mg-clays. Because dolomite and clay minerals are thought to be the primary sinks of magnesium in seawater on geologic timescales (Hardie, 1996; Holland and Zimmerman, 2000), estimates of magnesium isotope fractionation factors associated with the precipitation of these minerals under natural conditions are important for understanding how the magnesium isotopic composition of seawater may have changed over geologic time.

In this paper, we present the first magnesium isotopic data on pore-fluids from six ODP sites (925, 984, 1012, 1082, 1086, and 1219). We also present magnesium isotope data for six dolomite samples from sites 1082 and 1012. We use the data to identify sources and sinks of magnesium in deep-sea sediment pore-fluids. We show that similar magnesium concentration depth profiles are associated with different depth profiles in magnesium isotopes. Using a diffusion-reaction model of magnesium isotopes in deep-sea sediment pore-fluids, we estimate magnesium isotope fractionation factors associated with net magnesium addition to and/or removal from the pore-fluid. We discuss implications for magnesium isotope fractionation and magnesium cycling in deep-sea sediments.

1.1. Sample locations and description

ODP sites used in this study span a range of depositional settings and sediment types (Figs. 1 and 2). Cl^- content of the pore-fluid is similar at all sites and at all depths (538–575 mM), indicating that subsurface brines are not important. Sites 1082, 1086, and 1012 are located near upwelling regions on the western continental margin of Africa and North America, respectively (Lyle et al., 1997; Wefer et al., 1998). Sedimentation rates at these sites are rapid (average 4–12 cm/kyr) and cored intervals range in age from late Miocene to the late Pleistocene. Sediments at sites 1082, 1086, and 1012 are characterized by significant contributions from both biogenic and detrital sources. The biogenic component of the sediment is primarily $CaCO_3$, averaging 41–78 weight% (wt.%); contributions from siliceous organisms (diatoms, radiolarians, sponge spicules) are variable, but generally minor. The detrital component of the sediment at these sites is dominated by clay minerals (smectite, kaolinite, illite, and micas) with minor amounts of volcanic glass, feldspar, and quartz. Sediments at these sites also contain significant amounts of organic carbon (average 1.1–3.7 wt.%). Diagenetic reactions at these sites are dominated by organic carbon remineralization. Associated changes in the chemical composition of pore-fluids include rapid SO_4^{2-} depletion ($[SO_4^{2-}] = 0$ at 22, 28, and 182 m at sites 1082, 1012, and 1086, respectively) and high concentrations of NH_4^+ (maximum = 25.5, 15.2, and 2.8 mM at sites 1082, 1012, and 1086, respectively) and alkalinity (maximum = 75.6, 67.3, and 17.4 mEq at sites 1082, 1012, and 1086, respectively). Sites 1082 and 1012 also contain multiple cm-thick beds of dolomite at depths >120 m at site 1082 and >170 m at site 1012. Discrete dolomite beds are not observed in the cored sequence from site 1086.

Site 984 is a high-sedimentation-rate (average ~14 cm/kyr) pelagic sequence located on the Bjorn Drift on the eastern flank of the Reykjanes Ridge. Sediments at this site range in age from the late Pliocene to the Holocene and are composed primarily of fine-grained terrigenous silts and clays transported from Iceland (Jansen et al., 1996). The mineralogy of the clastic component is dominated by plagioclase, smectite, and quartz, with minor amounts of illite, kaolinite, and chlorite (Carter and Raymo, 1999). Carbonate and organic carbon contents at site 984 are low, averaging ~8 wt.% and <0.25 wt.%, respectively. However, because sedimentation rates are high, organic carbon accumulates rapidly and observed changes in pore-fluid chemistry are dominated by respiration, as indicated by the complete consumption of SO_4^{2-} ($[SO_4^{2-}] = 0$ mM at 120 m) and elevated concentrations of NH_4^+ (maxi-

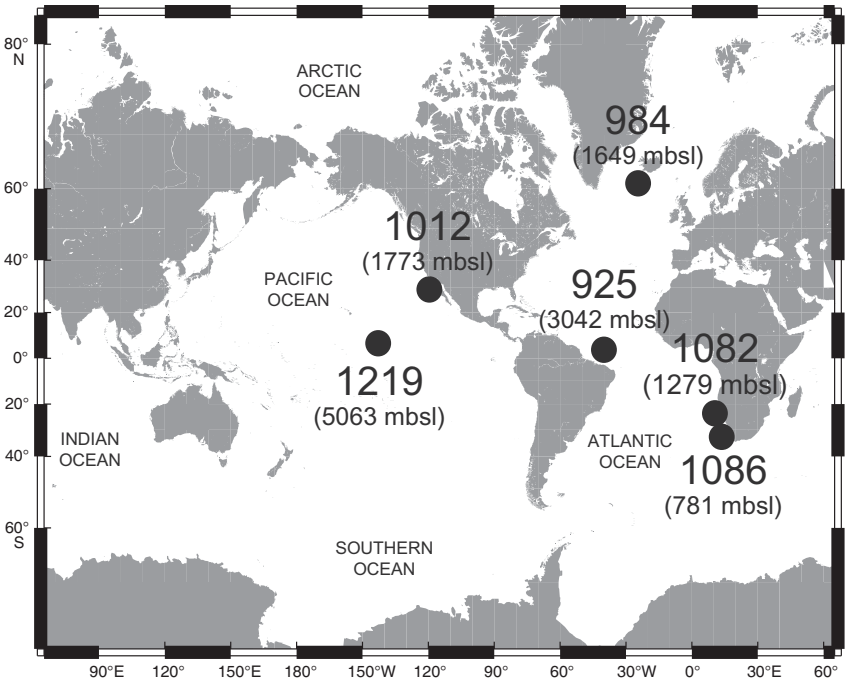

Fig. 1. ODP sites measured in this study. See text for further details.

mum = 3.1 mM at 290 m) and alkalinity (maximum = 11 mEq between 80 and 140 m).

Sites 925 and 1219 are located on the Ceara Rise in the western tropical Atlantic, and the central Pacific abyssal plain, respectively (Curry et al., 1995; Lyle et al., 2002). These sites are typical of deep-water pelagic sequences in that they are characterized by slow sedimentation rates (averaging 2.4 and <1 cm/kyr, respectively) and very low organic carbon contents (averaging 0.07 and 0.08 wt.%, respectively). Sediments at site 925 consist primarily of $CaCO_3$ (averaging 66 wt.%) with variable amounts of clay minerals. At site 1219, sediments consist primarily of nanofossil and radiolarian oozes with varying clay content. Highest clay contents occur in the upper 30 m (>50 wt.% smectite + illite), whereas the rest of the sequence is composed principally of $CaCO_3$ (average ~75 wt.% between 30 and 170 m) or opal (average ~70 wt.% between 170 and 230 m). In contrast to sites 1082, 1086, 1012, and 984, changes in the chemical composition of pore-fluids at sites 925 and 1219 are not dominated by the respiration of organic carbon. SO_4^{2-} concentrations decrease with depth, but the decline occurs over a much larger depth scale and non-zero sulfate concentrations are found in the deepest measured samples at both sites 1219 ($[SO_4^{2-}] =$ 26.6 mM at 200 m) and 925 ($[SO_4^{2-}] = 7.2$ mM at 740 m). Similarly, both NH_4^+ concentrations (maximum = 7 μM and 1.4 mM at sites 1219 and 925, respectively) and pore-fluid alkalinity (maximum = 3.1 and 10.6 mEq at sites 1219 and 925, respectively) remain relatively low at both sites.

1.2. Magnesium concentration profiles

Magnesium concentrations decrease down core at all sites, though the shape and magnitude of the decline varies (Fig. 2). Although large increases in the concentration of magnesium in seawater cannot be excluded as the reason for lower magnesium concentrations at depth (Fantle and DePaolo, 2006), the observed magnesium profiles have been interpreted to reflect net precipitation of Mg-minerals (dolomite and Mg-clays) in the sediment column and/or underlying basalt (Lawrence et al., 1975; Gieskes and Lawrence, 1981; Baker, 1985; Moore et al., 2004). Similarly, the transient increase in magnesium concentration observed at two sites (1082 and 1012; Fig. 2), indicates a local net magnesium source. Possible sources include the release of magnesium adsorbed to sediment–particle surfaces by ion exchange with pore-fluid NH_4^+ (Von Breymann and Suess, 1988; Vonbreymann et al., 1990), weathering of igneous minerals (Gieskes and Lawrence, 1981), and dissolution of carbonates (calcite and aragonite; Fantle and DePaolo, 2006). At sites 1082, 1086, and 1012, dolomite precipitation is thought to be the principal magnesium sink, at least in the upper portion of the sediment column (Lyle et al., 1997; Wefer et al., 1998; Moore et al., 2004). At these sites, the decline in magnesium is accompanied by a similar decline in calcium, consistent with dolomite precipitation. However, the ratio of the change in magnesium and calcium ($\Delta Mg/\Delta Ca$) varies significantly between sites, from +0.71 in the upper 50 m at site 1012 to +1.09 in the upper 40 m at site 1082 to +2.30 in the upper 100 m at site 1086 (Fig. 2a–c). The chemical composition of pore-fluids at these sites is also suggestive of dolomite precipitation as similar chemical conditions (high alkalinity, depleted in SO_4^{2-}) are associated with dolomite precipitation in a range of modern sedimentary systems (Baker, 1985; Vasconcelos and McKenzie, 1997; Mazzullo, 2000; Teal et al., 2000). Finally, the presence of multiple cm-thick beds of authigenic dolomite at sites 1082 and 1012 indicate once active dolomite precipitation in the sediment column at these sites.

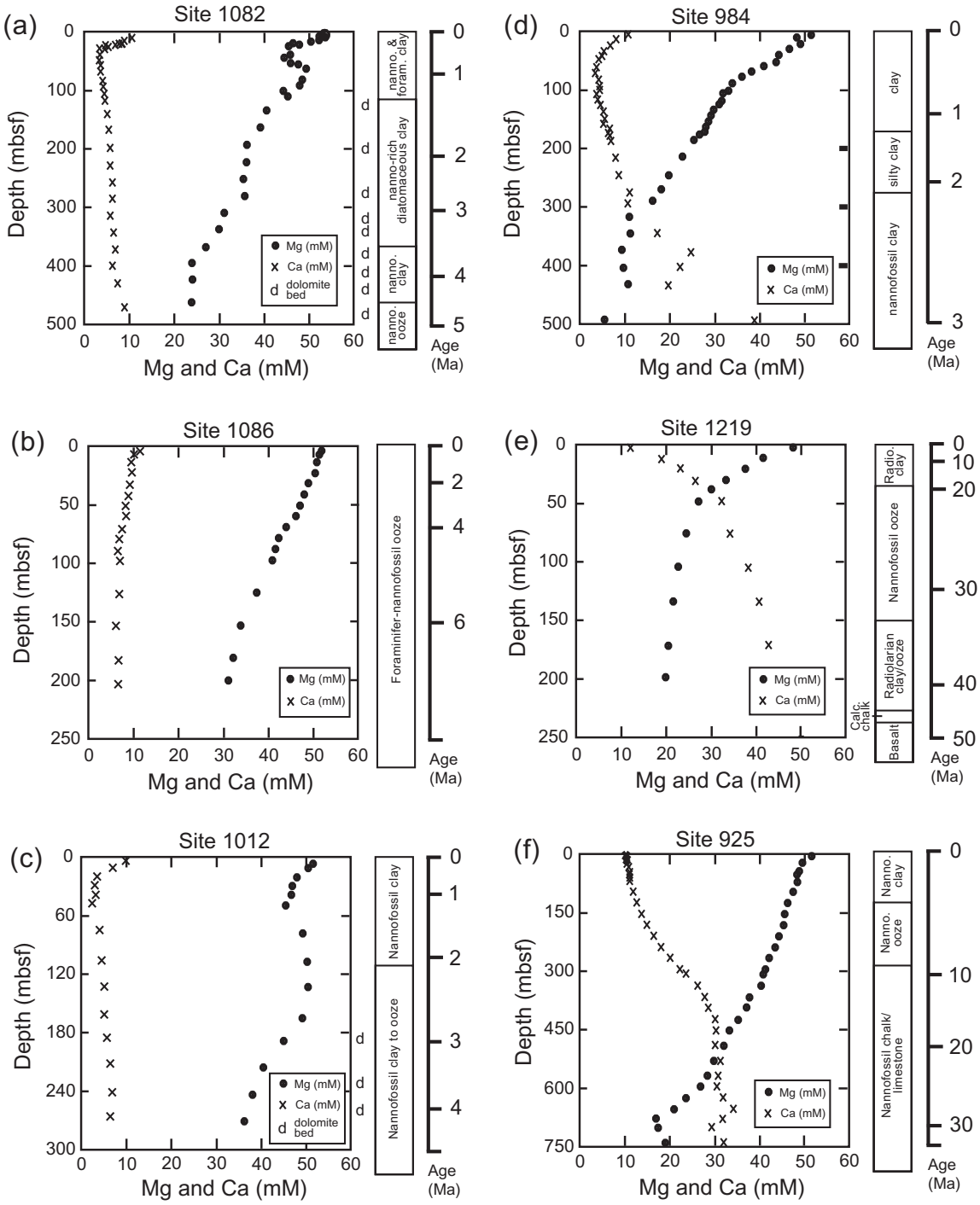

Fig. 2. Magnesium (•) and calcium (*x*) concentration profiles, lithologies, and sediment ages for the studied sites. See text for further details.

At sites 984, 925, and 1219, magnesium removal has been attributed to the precipitation of Mg-clay minerals (e.g., smectites) in the sediment column and/or underlying basalt (Curry et al., 1995; Jansen et al., 1996; Lyle et al., 2002). At site 1219, a nearly one to one relationship exists between changes in magnesium and calcium concentrations with depth ($\Delta Mg/\Delta Ca = -0.95$; Fig. 2e). At site 925, a similar relationship is observed; however, the decline in magnesium is ~50% larger than the increase in calcium ($\Delta Mg/\Delta Ca = -1.54$; Fig. 2f). Profiles of this type are thought to reflect submarine weathering of basalt (calcium source) and associated precipitation of clay minerals (magnesium sink) at low temperatures, an interpretation that is consistent with the observed decline in pore-water $\delta^{18}O$ values

(Lawrence et al., 1975; Schrag et al., 1996). Magnesium and calcium profiles at site 984 are similar in many respects to those associated with dolomite precipitation in the upper 70 m of the sediment column, where the decline in magnesium is accompanied by a decline in calcium ($\Delta Mg/\Delta Ca = +1.87$; Fig. 2d). Changes in pore-fluid chemistry (declining SO_{42-}, increasing alkalinity) at site 984 are also consistent with dolomite precipitation. However, the abundance of detrital basalt from Iceland, together with measured rates of mineral dissolution and precipitation from pore-fluid U isotopes (Maher et al., 2006) and lack of evidence for authigenic dolomite, suggest that the decline in magnesium at site 984 could also be due to low-temperature weathering of basalt and associated formation of Mg-clays within the sediment column.

2. METHODS

Precise and accurate magnesium isotope measurements using inductively coupled mass spectrometry (ICP-MS) require that contributions from molecular interferences, (e.g., CN^+), doubly-charged ions (e.g., $^{48}Ca^{2+}$), and species other than Mg that affect instrument fractionation (matrix effects (e.g., Ca, Na; Galy et al., 2001) be reduced. To reduce molecular interferences associated with species containing O, N, C, and H, samples are introduced to the mass spectrometer using an Elemental Scientific, Inc. Apex Q nebulizer fitted with an ACM membrane desolvator. To minimize contributions from doubly-charged ions and variations in the composition of the sample matrix, samples containing 2–4 μg of Mg were loaded in 1 N HNO_3 acid and passed twice through ion exchange columns (Bio-Rad X12 resin). Ultra-pure acids (VWR Omnitrace) and 18-Ω de-ionized water were used to assure small procedural blanks (<10 ng Mg or <0.33% of the sample size). Our column procedure efficiently separates magnesium from other cations and achieves yields that are >99%. Purity of separated samples was verified using a Thermo-Finnigan X-Series quadrupole ICP-MS with a H_2/He collision cell in the Laboratory of Geochemical Petrology at Harvard University. A dilution series of a multi-element standard was used to construct elemental calibration curves. Machine drift was corrected by interpolation from repeated analyses of the multi-element standards during a sample run. External errors (1σSD) from repeat analysis of a 10 ppb multi-element standard are <15% for all elements. Final cation (Na, Ca, Mn, Sr, Fe, Al, K)/Mg ratios for all samples measured for magnesium isotopes are <0.05 (g/g).

Pore-fluid samples were obtained from the Ocean Drilling Program and taken from 5- to 15-cm whole-round sections of the core while at sea (Sayles and Manheim, 1975). Collected pore-fluid samples were then passed through a 0.45-μm Gelman polysulfone filter and stored in glass ampules for later analyses. Major element compositions, salinity, pH, and alkalinity of the pore-fluid were all measured while at sea with a precision of 2–3%. Samples were centrifuged and diluted prior to ion exchange chromatography, but additional filtering was not required as the magnesium contents of the studied pore-fluids are high (tens of mM), making significant contamination from nanophases unlikely. The presence of dolomite in lithified samples from sites 1082 and 1012 was inferred from ODP reports (Lyle et al., 1997; Wefer et al., 1998; Pufahl and Wefer, 2001) and verified by XRD on a Scintag XDS 2000 diffractometer, using CuKα1 radiation at −40 kV and 30 mA at Harvard University. The non-carbonate fractions of the samples were high (>60 wt.%). Approximately 1 mg of powdered sample was dissolved in 12 mL of 0.1 N acetate-buffered acetic acid for 4 h at 25 °C to minimize the contribution of Mg from the non-carbonate fraction. The samples were then centrifuged for 20 min and the supernatant removed for Mg separation. Mg/Ca ratios of the dissolved sample range from 0.95 to 1.12 and are consistent with dolomite as the principle source of Mg. However, there is a small excess of magnesium of ~10% compared to stoichiometric dolomite in two samples, suggesting some contamination of non-dolomite Mg from ion exchange and/or dissolution of soluble clays. We consider the consequences of this contamination for the measured $\delta^{26}Mg$ values. Solid samples were also measured for carbon and oxygen isotopes on a VG Optima dual inlet mass spectrometer attached to a VG Isocarb preparation device in the Laboratory of Geochemical Oceanography at Harvard University. $\delta^{13}C$ and $\delta^{18}O$ values were calibrated to VPDB using the Cararra Marble standard. External errors (1σSD) of the measurements are typically < 0.1‰.

Magnesium isotopic analyses were carried out on a GV Isoprobe P multi-collector inductively coupled plasma mass spectrometer (MC-ICP-MS). Samples were diluted to 150 ppb Mg in 2% HNO_3 to give 1.5–3 V on mass 24. Data were acquired in blocks of 15–20 ratios of 10 s integration times. Internal reproducibility of $^{25}Mg/^{24}Mg$ and $^{26}Mg/^{24}Mg$ ratios was typically <0.1‰ and 0.2‰ (1σSD), respectively. Sample-standard-sample bracketing was used to correct for instrumental mass fractionation (e.g., Galy et al., 2001). Magnesium isotope ratios are reported using delta notation:

$$\delta^{25,26}Mg = \left(\frac{(^{25,26}Mg/^{24}Mg)_{SAM}}{(^{25,26}Mg/^{24}Mg)_{STD}} - 1\right) \times 1000$$

where $(^{25,26}Mg/^{24}Mg)$ is the measured $^{26}Mg/^{24}Mg$ ratio of the DSM-3 Mg standard (Galy et al., 2003). Repeat measurements of the Cambridge-1 Mg standard yielded $\delta^{25}Mg$ and $\delta^{26}Mg$ values of -1.32 ± 0.13‰ and -2.62 ± 0.25‰ (2σSD external; $n > 200$) relative to DSM-3, indistinguishable from published values ($\delta^{25}Mg = -1.33 \pm 0.07$‰; $\delta^{26}Mg = -2.58 \pm 0.14$‰, Galy et al., 2003). To verify that our sample procedure did not fractionate magnesium isotopes we compared measured $\delta^{26}Mg$ values of pure Mg standards to both pure and cation-spiked Mg standards that had been run through our ion exchange procedure (Table 1). In addition, repeat separation and isotopic analyses ($N = 5$) of seawater from Bermuda yielded $\delta^{25}Mg$ and $\delta^{26}Mg$ values of -0.41 ± 0.09‰ and -0.79 ± 0.18‰, respectively, indistinguishable from published values ($\delta^{25}Mg = -0.40 \pm 0.07$‰; $\delta^{26}Mg = -0.81 \pm 0.14$‰ (Galy et al., 2003). Plotted in three-isotope space ($\delta^{25}Mg$ vs. $\delta^{26}Mg$; Fig. 3) the samples measured in this study lie on a line with a slope of 0.527 ± 0.009 ($R^2 = 0.996$). This slope is very similar to that expected for equilibrium

Table 1
Measured and expected δ^{26}Mg values for magnesium isotope standards. HU-1 is a pure Mg solution spiked with equal amounts of Na, Ca, K, Al, Mn, Fe, and Sr. Analytical uncertainties are reported as the 2σ of repeat measurements on the MC-ICP-MS. *N*, number of total sample replicates; *n*, number of repeat measurements on the MC-ICP-MS.

Sample	δ^{26}Mg expected (‰)	δ^{26}Mg measured (‰)	2σ	*N*(*n*)
Cambridge-1	−2.58	−2.62	0.25	0(>200)
DSM-3	0.0	−0.02	0.04	1(4)
seawater	−0.82	−0.79	0.18	5(20)
spiked HU-1	−2.76	−2.81	0.27	4(16)

fractionation (0.521; Young and Galy, 2004) as well as previously published terrestrial fractionation slopes (0.513, Chang et al., 2004; 0.519, Young and Galy, 2004; Pogge von Strandmann, 2008; Huang et al., 2009), and demonstrates that the variability in magnesium isotopes that we observe is due to mass-dependent fractionation. For clarity, we present and discuss only δ^{26}Mg values.

3. NUMERICAL MODEL OF MAGNESIUM IN SEDIMENT PORE-FLUID

We developed a numerical model to quantify the cycling of magnesium in deep-sea pore-fluids. We use the model, together with measured magnesium concentration and δ^{26}Mg profiles to quantify rates of net magnesium cycling and try and identify net magnesium sources and sinks in the sediment column and underlying crust. We model the deposition of a sediment column and the chemical cycling of its pore-fluid using boxes of unconsolidated sediment, deposited at rates determined by the age and thickness of the sediment column, and compacted according to the observed porosity/depth relation (Richter and DePaolo, 1987; Richter and Depaolo, 1988; Schrag et al., 1992). We calculate down-core trends in magnesium concentrations and isotopes that result from reaction with the sediment and/or the underlying crust and transport by diffusion and advection. Initial conditions for the pore-fluid are acquired from the concentration and isotopic composition of magnesium in seawater at the time of sediment deposition. Boundary conditions for the model are the concentration and isotopic composition of magnesium in seawater through time (upper) and either zero-flux or finite-flux (lower), depending on the observed magnesium concentration profile at that site.

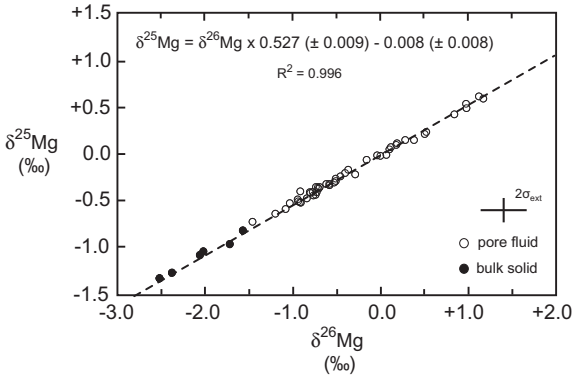

Fig. 3. Three isotope plot (δ^{25}Mg vs. δ^{26}Mg) for all samples measured in this study. The slope of 0.5271 (uncertainties define the 95% confidence envelope) is similar to published values and indicates mass-dependent behavior of magnesium isotope fractionation in this study.

Our model is based on a 1D diffusion–advection–reaction equation used by many authors (Berner, 1980; Richter and DePaolo, 1987; Schrag et al., 1992; Fantle and DePaolo, 2006):

$$\phi(z)\cdot\frac{\partial({}^{n}\mathrm{Mg})}{\partial t}=\frac{\partial}{\partial z}\left(\phi(z)\cdot D_{n_{Mg}}\cdot\frac{\partial {}^{n}\mathrm{Mg}(z)}{\partial z}\right)-\frac{\partial}{\partial z}(\phi(z)\cdot\omega(z)\cdot {}^{n}\mathrm{Mg}(z))-\phi(z)\cdot R_{n_{\mathrm{Mg}}}(z) \quad (1)$$

where ^{n}Mg is the concentration of ^{24}Mg, ^{25}Mg, or ^{26}Mg in mass per unit volume of pore-fluid, z is depth below the sediment–water interface, $D_{n_{\mathrm{Mg}}}$ is the depth-dependent bulk sediment diffusion coefficient ($m^2\,yr^{-1}$) for ^{24}Mg, ^{25}Mg, or ^{26}Mg, ϕ is the depth-dependent but time-invariant porosity, ω is the advective velocity ($m\,yr^{-1}$), and $R_{n_{\mathrm{Mg}}}$ is a source-sink term for ^{24}Mg, ^{25}Mg, or ^{26}Mg ($mol\,Mg\,m^{-3}\,yr^{-1}$). Porosity (ϕ) is obtained from fits to observed porosity profiles at each site. Bulk diffusion coefficients for magnesium ($D_{n_{\mathrm{Mg}}}$) depend on temperature and tortuosity. The effect of temperature on $D_{n_{\mathrm{Mg}}}$ is modeled after Boudreau (1997) using observed temperature profiles or geothermal gradients. Tortuosity is taken into account following Boudreau (1997) where $D_{n_{\mathrm{Mg}}}=\frac{D^{o}_{n_{\mathrm{Mg}}}}{\theta^2}$ and $D^{o}_{n_{\mathrm{Mg}}}$ is the diffusion coefficient for magnesium in solution (Li and Gregory, 1974). Tortuosity (θ) is related to porosity (ϕ) by the function: $\theta^2=1-ln(\phi^2)$ (Boudreau, 1997). Richter et al. (2006) showed that magnesium isotopes are not significantly fractionated during diffusion ($\alpha^{26/24}_{\mathrm{diffusion}}=1.00006$). As a result, we use a single diffusion coefficient for ^{24}Mg, ^{25}Mg, and ^{26}Mg. Sediment compaction decreases sediment porosity and drives pore-fluid toward the sediment–water interface. These advective velocities (ω) are calculated for each site using observed porosity profiles and sedimentation rates. At each time step where a unit of sediment is added, compaction of the other sediment layers is calculated and the reduction in pore space is converted into a flux of pore-fluid that is oriented towards the sediment–water interface. At all other time steps, advection of the pore-fluid is zero. Other sources of advection (e.g., hydrothermal convection) are assumed to be minor at sites 1082, 1086, 1012, 925, and 984 due to the thickness and/or clay content of the sediment cover (Anderson and Langseth, 1977; McDuff, 1981). External fluid flow is considered at site 1219, where the sediment cover is relatively thin (240 m).

The reaction term, $R_{n_{\mathrm{Mg}}}$, is a tunable model parameter that reflects the net addition/removal of magnesium from the pore-fluid. Each unit of sediment is associated with a value of $R_{n_{\mathrm{Mg}}}$ for each isotope of magnesium. We assume that the magnitude of $R_{n_{\mathrm{Mg}}}$ is a function of depth below

the sediment–water interface (and hence sediment age) and that values of $R_{n_{Mg}}$ are time-invariant for each depth interval. Our treatment of $R_{n_{Mg}}$ differs from previous studies (Richter and DePaolo, 1987, 1988; Fantle and DePaolo, 2006, 2007) in that we do not assume a particular form of the reaction rate expression with depth/age. We do this for three reasons: (1) the precipitation of diagenetic minerals can be localized at discrete boundaries in the sediment column that may migrate in response to changes in sediment composition (Meister et al., 2007, 2008), (2) sediments at the studied sites are heterogeneous in composition so multiple sources/sinks may be expected, and (3) we have few constraints on gross rates of magnesium cycling. A consequence of our approach is that $R_{n_{Mg}}$ does not reflect the uptake/loss of magnesium from an individual mineral phase but rather the net change in magnesium resulting from all precipitation, dissolution, and exchange reactions. Using a simple iterative routine, we tune $R_{n_{Mg}}$ at each depth interval for each isotope (e.g., $R_{24_{Mg}}$, $R_{25_{Mg}}$, and $R_{26_{Mg}}$) to fit both the magnesium concentration and isotope depth profiles. The quality of the model fit is evaluated by visual inspection. Using the tuned reaction rates of ^{25}Mg, ^{26}Mg, and ^{24}Mg as a function of depth, we calculate the ratio of the isotopic composition of the flux to that of the fluid as well as the average isotopic composition of net magnesium sources ($\delta^{26}Mg_{source}$). The ratio of the isotopic composition of the flux to the fluid can be understood as an empirical isotopic fractionation factor associated with net magnesium uptake/addition:

$$\varepsilon_{s-f}^{26/24} = 1000 \cdot \left(\alpha_{s-f}^{26/24} - 1\right), \quad (2)$$

$$\text{where } \alpha_{s-f}^{26/24} = \frac{R_{26_{Mg}}}{R_{24_{Mg}}} \cdot \left(\frac{^{24}Mg}{^{26}Mg}\right)_{\text{pore-fluid}}$$

It is important to emphasize that the fractionation factors calculated by the model reflect the summed isotopic effect of all local precipitation, dissolution, and exchange reactions. This is because the isotopic composition of magnesium in the pore-fluid depends on the gross fluxes of magnesium through the pore-fluid. In contrast, changes in magnesium concentrations with depth (and hence the modeled reaction rates) reflect only the net uptake/addition of magnesium. This difference complicates our interpretation of the modeled magnesium isotope fractionation factors and is explored in detail in the discussion.

We solve Eq. (1) for each isotope of magnesium (^{24}Mg, ^{25}Mg, and ^{26}Mg) using an explicit finite difference formula for an uneven grid (Pearson, 1968). Grid spacing reflects the change in sediment thickness with depth due to compaction. As a result, the vertical resolution of the model increases with depth as sediments with uniform initial thickness are compacted according to the observed the porosity–depth relation. The thickness of units of un-compacted sediment at the studied sites ranges from 6.9 to 26.6 m. Increasing the vertical resolution of the grid (i.e., depositing smaller units of sediment more frequently) by a factor of three does not significantly change the results presented here. Time steps (Δt) are chosen to avoid numerical instability (Boudreau, 1997) and range from 210 to 2000 yrs. The total number of time steps that the model is run is determined by the age of the sediment column at each site (see Fig. 2). Boundary conditions are prescribed at the sediment–water interface and the bottom of the cored sediment column. The magnesium concentration and isotopic composition at the sediment–water interface are set constant at the values for modern seawater ([Mg] = 53 mM, $\delta^{25}Mg = -0.41‰$ and $\delta^{26}Mg = -0.79‰$). Boundary conditions at the bottom of the sediment column are either zero $\left(\frac{dMg}{dz}|_{z_{end}} = 0\right)$ or constant $\left(\frac{dMg}{dz}|_{z_{end}} = \text{const.}\right)$ flux, depending on the magnesium concentration profile at each site.

4. RESULTS

Pore-fluid magnesium isotope data measured in this study are presented in Table 2. At all sites, measured $\delta^{26}Mg$ profiles show systematic trends with depth. At sites 1012, 1082, and 1086, $\delta^{26}Mg$ values increase with depth by 1.25–2‰. For example, at site 1082, $\delta^{26}Mg$ values increase from −0.74‰ at 1.4 m to +1.03‰ at 461.6 m. Similar increases in $\delta^{26}Mg$ values are observed at sites 1086 (−0.74‰ at 1.4 m to +0.59‰ at 201.1 m) and 1012 (−0.77‰ at 3 m to +1.13‰ at 267.1 m). In contrast, at sites 925, 1219, and 984 pore-fluid $\delta^{26}Mg$ values decrease with depth. The decrease in $\delta^{26}Mg$ values at sites 1219 and 925 is small (0.1–0.2‰), from −0.71‰ at 3 m to −0.91‰ at 200.5 m and −0.59‰ at 3 m to −0.72‰ at 424 m, respectively. A larger decline in $\delta^{26}Mg$ values (1.9‰) is observed at site 984, from −0.75‰ at 9.6 m to −2.62‰ at 271 m. The magnesium isotopic composition of measured dolomite samples from sites 1082 and 1012 are also presented in Table 1. At site 1082, $\delta^{26}Mg$ values for dolomite range from −2.02‰ at 128.6 m below seafloor (mbsf) and −2.06‰ at 199.7 mbsf to −1.72‰ at 327.5 mbsf. At site 1012, dolomite samples are slightly more depleted, with $\delta^{26}Mg$ values ranging from −2.52‰ at 169–170 mbsf to −2.38‰ at 244.9 mbsf.

Modeled magnesium concentration and $\delta^{26}Mg$ profiles are shown in Figs. 4 and 5. At all sites, declining magnesium concentrations with depth can be explained by net precipitation of Mg-minerals in the sediment column and/or underlying basalt. Excursions towards higher magnesium concentrations at sites 1082 and 1012 suggest a local net magnesium source within the sediment column. Modeled rates of net magnesium uptake/addition from/to the pore-fluid range from $<10^{-6}$ to 10^{-4} mol Mg m^{-3} yr^{-1}. These rates are small and suggest that the net contribution of newly precipitated Mg-minerals will be small compared to the mass of sediment. For example, dolomite precipitation at a rate of 10^{-4} mol Mg m^{-3} yr^{-1} would have to be maintained for ~19 million years to fully cement sediment with an initial porosity of 70%. As these rates are likely maintained for only a fraction of this time (i.e., the residence time of sediment in the depth interval associated with those high rates), authigenic minerals are expected to make only a small net contribution (<5 wt.%) to the bulk sediment. In light of these slow precipitation rates, the formation of the thick (up to 10's of centimeters) layers of dolomite at sites 1082 and 1012 seems problematic. One possibility is that a large fraction of the magnesium precipitated in the dolomite is

Table 2
Measured δ^{26}Mg values for pore-fluids and dolomite samples from studied sites. Analytical uncertainties are reported as the 2σ of repeat measurements on the MC-ICP-MS. *N*, number of total sample replicates; *n*, number of repeat measurements on the MC-ICP-MS.

Sample	Depth (mbsf)	[Mg] (mM)	δ^{26}Mg (‰)	2σ	*N*(*n*)	Sample	Depth (mbsf)	[Mg] (mM)	δ^{26}Mg (‰)	2σ	*N*(*n*)
Seawater	0	53	−0.81	0.13	5(20)						
Pore-fluid						*Pore-fluid*					
Site 1082	1.4	53.43	−0.74	0.17	2(7)	Site 984	9.6	47.9	−0.75	0.27	1(5)
	4.4	52.19	−0.74	0.15	1(3)		30.1	46.3	−0.92	0.03	1(2)
	7.5	52.52	−0.85	0.25	1(3)		49.1	43	−0.95	0.17	1(4)
	20	46.13	−0.29	0.07	1(3)		68.1	37.8	−0.94	0.22	1(5)
	40.4	44.41	0.07	0.01	1(2)		96.6	32.7	−1.04	0.17	1(5)
	54.1	46.86	0.19	0.15	1(4)		153.6	28.2	−1.20	0.20	1(6)
	97.5	44.23	0.38	0.24	1(3)		185.5	24.9	−1.46	0.24	1(5)
	160	39.06	0.86	0.25	1(4)		271.0	17.7	−1.57	0.06	1(6)
	365	26.89	0.97	0.30	1(3)		346.2	10.8	−2.07	0.25	1(5)
	461.6	23.51	1.03	0.05	1(2)		498.5	5.3	−2.56	0.18	1(3)
Site 1086	1.4	52.4	−0.74	0.18	1(4)	Site 1219	3.0	48.6	−0.71	0.09	1(6)
	20.6	50.71	−0.57	0.11	1(5)		39.0	30.4	−0.77	0.18	1(6)
	39.6	47.97	−0.51	0.07	1(5)		48.5	27.5	−0.73	0.08	1(3)
	58.6	45.84	−0.41	0.16	1(4)		105.5	22.9	−0.84	0.25	1(6)
	77.5	41.87	−0.37	0.03	1(4)		200.5	20.1	−0.91	0.14	1(3)
	153.6	33.7	0.15	0.17	1(4)						
	182.1	31.75	0.32	0.17	1(5)	Site 925	3.0	51.75	−0.59	0.17	1(6)
	201.1	30.5	0.59	0.18	1(4)		46.5	48.91	−0.53	0.13	1(4)
							94.5	47.75	−0.51	0.19	1(6)
							293.9	41.38	−0.58	0.03	1(3)
Site 1012	3.0	51.3	−0.77	0.26	1(3)		336.0	40.51	−0.70	0.22	1(6)
	28.2	47.1	−0.41	0.09	1(6)		424.0	35.36	−0.72	0.07	1(3)
	47.2	45.7	−0.04	0.17	1(6)						
	75.7	49.3	−0.16	0.18	1(6)						
	104.3	50.2	0.12	0.13	2(11)	*Dolomite*					
	131.4	50.4	0.00	0.19	1(6)	Site 1082	128.6		−2.02	0.17	1(4)
	161.7	49.2	0.18	0.07	1(5)		199.7		−2.06	0.21	1(5)
	211.8	40.7	0.56	0.18	1(5)		327.5		−1.72	0.21	1(4)
	240.5	37.9	0.98	0.08	1(6)						
	267.1	36.6	1.13	0.14	1(4)	Site 1012	169.9		−2.52	0.26	1(5)
							170		−2.52	0.23	1(3)
							244.9		−2.38	0.26	1(6)

sourced locally (i.e., from the surrounding sediment and not from seawater). However, comparisons between the modeled fractionation factor and estimates of the fractionation factor from the δ^{26}Mg value of the dolomite itself suggest that the vast majority of the magnesium in the dolomite is derived from seawater (i.e., local exchange reactions are minor – see Section 5). A more likely explanation for the massive layers of diagenetic dolomite is that they reflect periods when the sulfate–methane interface shoaled dramatically and/or remained fixed at a particular depth due to changes in the composition of deposited sediments under conditions of non-steady state diagenesis (Meister et al., 2007, 2008). Reaction rates explicitly linked to the composition of deposited sediments are not explored here, though it may be appropriate to investigate this in future models.

Modeled magnesium isotope fractionation factors ($\varepsilon_{s-f}^{26/24}$) range from −2.7‰ to +1.25‰ and vary systematically between sites (Table 3 and Figs. 4, 5). At sites where the decline in magnesium concentrations in the pore-fluid is thought to reflect dolomite precipitation (1082, 1086, and 1012), the modeled net magnesium sinks in the upper part of the sediment columns are significantly depleted in ^{26}Mg relative to the pore-fluid ($\varepsilon_{s-f}^{26/24} = -2.0‰$ to −2.7‰; Fig. 4). In contrast, at sites where magnesium cycling is thought to reflect alteration of the underlying crust (1219 and 925), the modeled net magnesium sinks are slightly enriched in ^{26}Mg ($\varepsilon_{s-f}^{26/24} = 0.0‰$ to +1.25‰; Fig. 5). Similarly, the observed increase in $\varepsilon_{s-f}^{26/24}$ with depth at site 1082 may also indicate increased precipitation of clay minerals at greater depths. At site 984, where the identity of the magnesium sink is more ambiguous, the observed increase in the δ^{26}Mg values of the pore-fluid is consistent with a net magnesium sink both within and below the cored sediment column that is 0.95‰ to 1.25‰ enriched in ^{26}Mg. Although only sites 1082 and 1012 are characterized by a net magnesium source within the sediment column, modeled δ^{26}Mg values of these sources are similar, at 0.0‰ to −0.2‰.

We examine the sensitivity of modeled δ^{26}Mg profiles to estimates of $\varepsilon_{s-f}^{26/24}$ by varying the modeled fractionation factors at each site by ±0.5‰. As shown in Figs. 4 and 5, the analytical uncertainties of our measured δ^{26}Mg profiles translate into uncertainties of ~±0.5‰ for modeled fractionation factors and values of $\delta^{26}Mg_{source}$ (Figs. 4 and 5). Reactions near the seafloor have somewhat larger

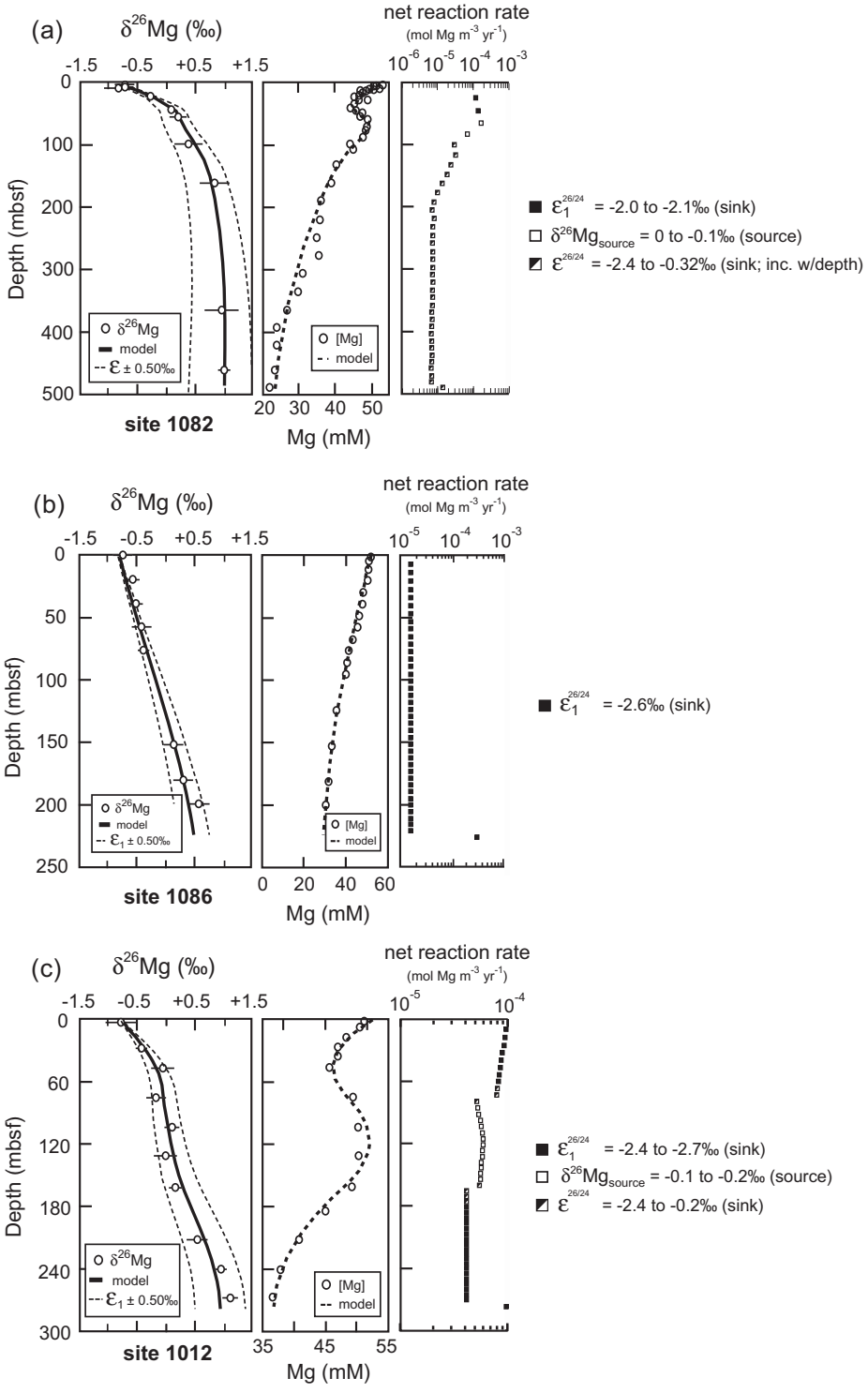

Fig. 4. (a–c) Measured magnesium isotope (δ^{26}Mg) profiles and modeled [Mg] and δ^{26}Mg profiles for sites 1082, 1086, and 1012. δ^{26}Mg data for each site can be found in Table 1. Model fits are indicated by the solid lines (—). At each site, net reaction rates (R_{model}) for ^{24}Mg, ^{25}Mg, and ^{26}Mg are tuned to fit both concentration and isotope profiles. Each source/sink of magnesium is associated with an isotopic fractionation ($\varepsilon^{26/24}$) or composition (δ^{26}Mg), indicated by the color of the reaction rate bar. Uncertainties in modeled fractionation factors ($\varepsilon_1^{26/24}$) are calculated by varying all fractionation factors by ±0.5‰ and is indicated by the dotted lines (- - -). (R_{model}) at the bottom of the modeled sediment column is the lower boundary condition and reflects the summed net reaction rate for all of the sediment/crust underlying the modeled sediment column.

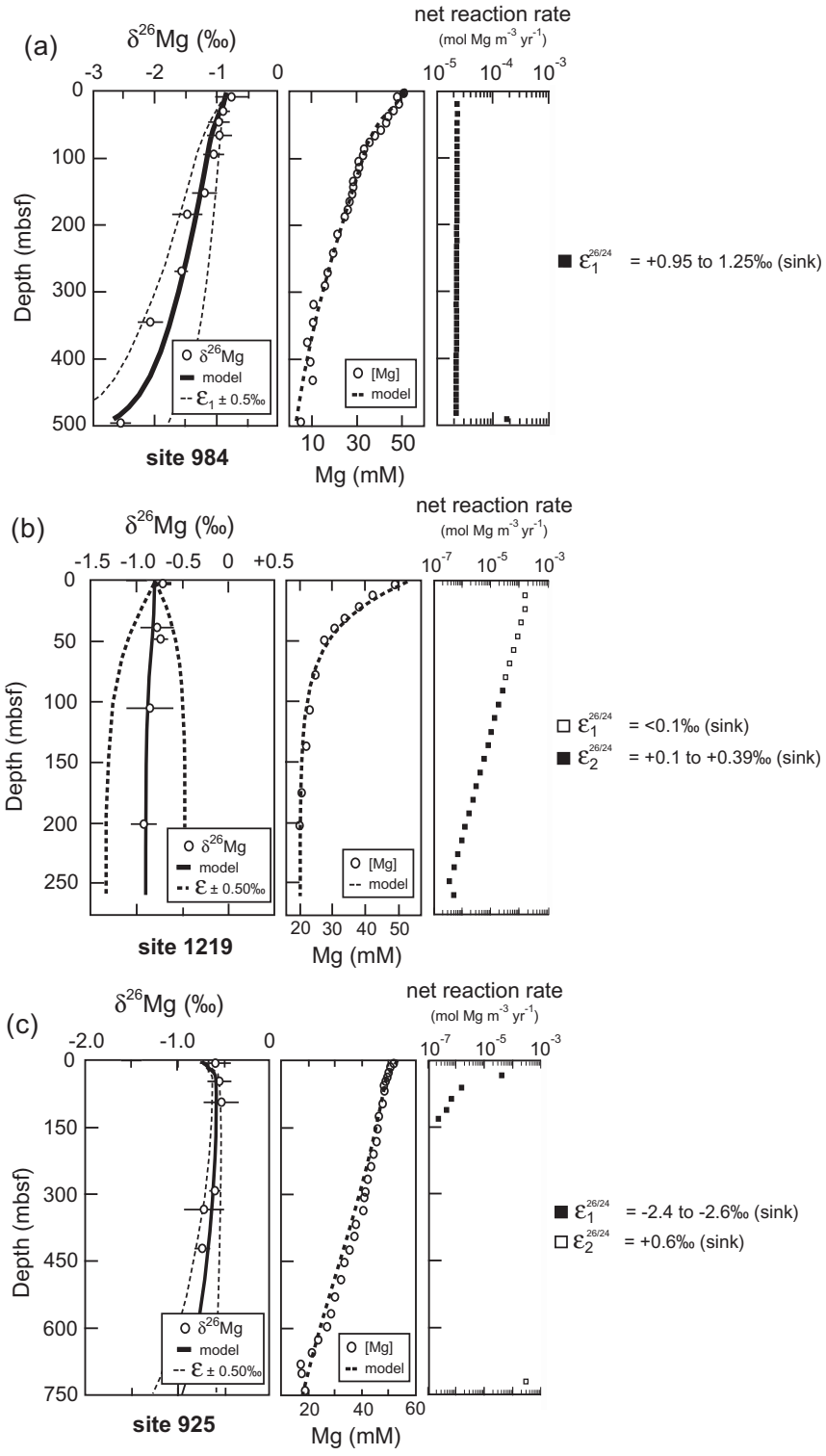

Fig. 5. (a–c) Measured magnesium isotope ($\delta^{26}Mg$) profiles and modeled [Mg] and $\delta^{26}Mg$ profiles for sites 984, 1219, and 925. $\delta^{26}Mg$ data for each site can be found in Table 1. Model fits are indicated by the solid lines (—). At each site, net reaction rates (R_{model}) for ^{24}Mg, ^{25}Mg, and ^{26}Mg are tuned to fit both concentration and isotope profiles. Each source/sink of magnesium is associated with an isotopic fractionation ($\varepsilon^{26/24}$) or composition ($\delta^{26}Mg$), indicated by the color of the reaction rate bar. Uncertainties in modeled fractionation factors ($\varepsilon^{26/24}$) are calculated by varying all fractionation factors by ±0.5‰ and is indicated by the dotted lines (- - -). (R_{model}) at the bottom of the modeled sediment column is the lower boundary condition and reflects the summed net reaction rate for all of the sediment/crust underlying the modeled sediment column.

Table 3
Measured $\delta^{26}Mg$ values, Mg/Ca ratios, $\delta^{13}C$ values, and $\delta^{18}O$ values for dolomite samples from sites 1082 and 1012.

Site	Depth (mbsf)	Mg/Ca (mol/mol)	$\delta^{13}C$ (‰)	$\delta^{18}O$ (‰)	$\delta^{26}Mg$ (‰)
1082	128.6	1.05	11.50	4.13	−2.02
1082	199.7	1.04	13.40	5.68	−2.06
1082	327.5	1.00	5.65	5.38	−1.72
1012	169.9	1.11	5.59	5.20	−2.52
1012	170	1.12	3.62	4.17	−2.52
1012	244.9	0.95	12.58	6.07	−2.38

uncertainties in estimated fractionation factors due to buffering of pore-fluid $\delta^{26}Mg$ values by the overlying seawater. Uncertainties in model parameters that change the distribution and/or relative magnitude of modeled magnesium fluxes ($R_{n_{Mg}}$), such as rates of external fluid flow and the effect of tortuosity on $D_{n_{Mg}}$, may also contribute to uncertainties in $\varepsilon_{s-f}^{26/24}$ and $\delta^{26}Mg_{source}$. However, model calculations using alternative parameterizations of tortuosity and diffusion in sedimentary systems (see Boudreau, 1997) suggest that the effect on estimated values of $\varepsilon_{s-f}^{26/24}$ and $\delta^{26}Mg_{source}$ is small. In addition, rates of external fluid flow at sites 1082, 1086, 1012, 984, and 925 are likely low due to the hydraulic resistance provided by a thick (>300 m) sediment column (Anderson and Langseth, 1977).

At site 1219, a thin sediment column (240 m), 50% of which is permeable carbonate ooze, may support high rates of fluid flow. Although the abundance of smectite (bulk sediment = 2–3 wt.% Mg; (Lyle et al., 2002)) and presence of volcanic glass (trace to 3 wt.%) suggest that the modeled magnesium sink in the upper ~25 m of the sediment column (assuming no external flow; Fig. 5b) may be real, we explore the possibility that the magnesium profile at site 1219 can be explained by a single magnesium sink in the underlying basalt. Model calculations indicate that a single magnesium sink in the underlying basalt is consistent with the magnesium profiles at site 1219 if rates of upward (basalt to seafloor) fluid flow are ~0.04 cm/yr. This rate is faster than rates of advection due to sediment compaction (~0.01–0.001 cm/yr), but significantly lower than estimates of convective fluid flow (10–100 cm/yr) based on measured curvilinear temperature-depth profiles at sites with thin (<100 m) sediment cover (Anderson and Langseth, 1977). Including external fluid flow at site 1219 has two effects on estimated values ε_{s-f}. First, it eliminates the fractionation factor associated with the magnesium sink within the sediment column. Second, the value of ε_{s-f} associated with the magnesium sink in the underlying basalt decreases from +0.39‰ to +0.21‰.

4.1. Magnesium isotopic composition of dolomites from site 1082 and 1012

The $\delta^{26}Mg$ values of dolomite samples from sites 1082 and 1012 are all isotopically depleted relative to the pore-fluid, with $\delta^{26}Mg$ values ranging from −2.06‰ to −2.52‰ (Table 4). $\delta^{13}C$ values for the samples are all significantly enriched relative to seawater (+3.62‰ to +13.40‰), consistent with formation in the zone of methanogenesis where the $\delta^{13}C$ of dissolved inorganic carbon (DIC) is elevated due to the production of isotopically depleted CH_4. $\delta^{18}O$ values for the samples range from 4.17‰ to 6.07‰ and are similar to diagenetic dolomites measured elsewhere (Meister et al., 2008). The small Mg excess observed in some

Table 4
Summary of estimated fractionation factors and $\delta^{26}Mg$ values of sources. Range of estimated fractionation factors for measured dolomite samples is related to the uncertainty in the $\delta^{26}Mg$ value of the precipitating solution. * Indicates model results when external fluid flow is considered.

Site	Depth (mbsf)	Type	Mg-carbonates		Mg-clays	Mg-source
			est · $\varepsilon^{26/24}$ (‰)	$\delta^{26}Mg$ (‰)	est · $\varepsilon^{26/24}$ (‰)	est · $\delta^{26}Mg$ (‰)
1082	0–50	Pore-fluid	−2.0 to −2.2			
	>100	Pore-fluid	−2.4			
	128.6	Solid	−1.7 to −2.2	−2.02		
	199.7	Solid	−1.8 to −2.3	−2.06		
	327.5	Solid	−1.4 to −1.9	−1.72		
	60 to 100	Pore-fluid				0.0 to −0.1
1012	0–70	Pore-fluid	−2.4 to −2.5			
	>180	Pore-fluid	−2.4 to −2.7			
	169.9	Solid	−2.2 to −2.7	−2.52		
	170	Solid	−2.2 to −2.7	−2.52		
	244.9	Solid	−2.1 to −2.6	−2.38		
	90–180	Pore-fluid				−0.1 to −0.2
1086	0 to >200	Pore-fluid	−2.6			
984	0 to >500	Pore-fluid			+0.92 to +1.25	
1219	0–80	Pore-fluid			<0.1 none*	
	80 to >240	Pore-fluid			+0.1 to +0.4 +0.21*	
925	0–150	Pore-fluid	−2.4 to −2.6			
	>750	Pore-fluid			+0.6	

of the samples may be due to contamination from associated clay minerals. Assuming a δ^{26}Mg value of clays of ~0‰, correcting for this contribution would yield dolomites that are slightly more depleted in δ^{26}Mg (0.1–0.25‰).

5. DISCUSSION

Our results show that the isotopic composition of magnesium in deep-sea pore-fluids exhibits systematic and reproducible behavior characterized by trends of both increasing and decreasing δ^{26}Mg values with depth. Because, at all sites, magnesium concentrations decline with depth, the simplest explanation for our data is that the differences between the δ^{26}Mg profiles at the studied sites reflect differences in the identity of the Mg-minerals that are precipitating in the sediment column and/or underlying crust. In this context the increase in the δ^{26}Mg values of the pore-fluid at sites 1082, 1086, and 1012 can be explained by the precipitation of a Mg-mineral, presumably dolomite, that is depleted in δ^{26}Mg relative to the pore-fluid by −2.0‰ to −2.7‰. Although the magnesium isotope fractionation factor associated with the precipitation of authigenic dolomite is not well known, modeled fractionation factors are broadly similar to fractionation factors reported in previous work on magnesium isotopes in dolomite as well as carbonate minerals more generally (e.g., −0.49‰ to −4.5‰; (Galy et al., 2002; Chang et al., 2004; Carder et al., 2005). In addition, the modeled δ^{26}Mg values of magnesium sources at sites 1082 and 1012 are consistent with the δ^{26}Mg values of silicate and clay minerals (e.g., 0‰ to −0.3‰; Young and Galy, 2004; Tipper et al., 2006a; Teng et al., 2007; Pogge von Strandmann, 2008). Similarly, the decrease in δ^{26}Mg values observed at sites 1219, 925, and 984 could be explained by the precipitation of Mg-clays that are enriched in δ^{26}Mg relative to the pore-fluid by 0‰ to +1.25‰. This is consistent with the observation that most published δ^{26}Mg values of clay minerals and shales are slightly enriched in δ^{26}Mg relative to primary silicates ($\delta^{26}Mg_{clay} - \delta^{26}Mg_{silicate} \sim +0.3$ to 0.5‰; (Young and Galy, 2004; Tipper et al., 2006a; Teng et al., 2007), though some have argued the opposite based on studies of Mg isotopes in weathered basaltic terrains (Pogge von Strandmann et al., 2008).

Although this straightforward interpretation of our data is consistent with previously published studies of magnesium isotopes in Mg-carbonates and Mg-clays, it makes two critical assumptions about the modeled net fractionation factors. First, it assumes that changes in the δ^{26}Mg values of the pore-fluid can be directly related to the net flux of magnesium to/from the pore-fluid calculated from the concentration profile. If there is significant local exchange of magnesium between sediment and pore-fluid, for example, due to recrystallization of dolomite, our modeled magnesium fluxes will underestimate the actual fluxes of magnesium through the pore-fluid. Second, it assumes that each net source/sink reflects a single Mg-mineral. We explore these assumptions for the studied sites below.

The interpretation of modeled magnesium isotope fractionation factors in deep-sea pore-fluids depends on two factors: (1) how much more magnesium moves through the pore-fluid than is indicated by our modeled net reaction rates, and (2) how many isotopically-distinct Mg-minerals are involved. Potential sources of this additional magnesium cycling are local exchange between sediment and pore-fluid, either by the recrystallization of a single mineral (e.g., calcite; Richter and DePaolo, 1987, 1988; Fantle and DePaolo, 2006, 2007) or the coupled dissolution/precipitation of different minerals (e.g., weathering of Mg-silicates to Mg-clays and carbonates). If the flux of magnesium through the pore-fluid is dominated by these local exchange reactions, changes in the magnesium isotopic composition of the pore-fluid with depth will depend on the combined effect of the isotopic composition of the magnesium source and any isotopic fractionation associated with magnesium removal. In this case, additional information on gross rates of magnesium cycling is needed to define a unique solution for the system and determine the real magnesium isotopic fractionation factors associated with mineral precipitation. In contrast, if the flux of magnesium through the pore-fluid is equal to or only slightly higher than the modeled net reaction rates, changes in the magnesium isotopic composition of the pore-fluid with depth will depend primarily on the isotopic composition of the dissolving solid or any isotopic fractionation associated with precipitation. In this case, the modeled isotopic fractionation factor will accurately reflect the δ^{26}Mg value of the dissolving solid or the real fractionation factor for mineral precipitation (assuming the system can be described by the dissolution or precipitation of a single mineral).

For most of the studied sites, constraints on gross rates of magnesium cycling are lacking and the best we can do is to assume that the contribution from local exchange reactions is small and examine how contributions from potential local exchange reactions would affect our interpretation of the modeled magnesium isotopic fractionation factors. At sites 1082 and 1012, we can derive an independent estimate of the fractionation factor associated with dolomite precipitation from the isotopic composition of the dolomite itself (δ^{26}Mg, δ^{13}C). By comparing this estimate with our model-derived fractionation factors we can place some constraint of the importance of local exchange reactions at these sites.

5.1. Comparing modeled fractionation factors at sites 1082 and 1012 to estimates from the δ^{26}Mg of authigenic dolomites

The δ^{26}Mg values of authigenic dolomites from sites 1082 and 1012 provide an independent measure of magnesium isotope fractionation during dolomite precipitation, though there are uncertainties because the δ^{26}Mg value of the pore-fluid from which the dolomite precipitated is unknown. As the δ^{26}Mg values of the pore-fluid increase with depth at both sites, the δ^{26}Mg value of modern seawater ($\delta^{26}Mg = -0.79$‰) represents a conservative minimum estimate for the δ^{26}Mg value of the precipitating fluid. Additional information on the likely δ^{26}Mg value of the precipitating fluid can be gleaned from the δ^{13}C values of the dolomites, which range from +3.62‰ to +13.40‰ (Table 3). These δ^{13}C values require that precipitation occurred in the zone of methanogenesis (Meister et al., 2007, 2008). At present at site 1082, the zone of enriched δ^{13}C of DIC occurs below 50 mbsf (Moore et al., 2004).

A similar or even shallower depth range is likely for site 1012 based on the pore-fluid SO_4^{2-} and CH_4 profiles, though the $\delta^{13}C$ of pore-fluid DIC at this site has not been measured. At these depths, the $\delta^{26}Mg$ of the pore-fluid is 0.5–1.0‰ heavier than seawater. Although the mass of dolomite in these layers suggests that the depth where the dolomite layers formed was likely much closer to the sediment–water interface, assuming that the relationship between the $\delta^{13}C$ value of the DIC and the $\delta^{26}Mg$ value of the pore-fluid was similar when these units precipitated, we calculate fractionation factors for dolomite precipitation that range from −1.4‰ to −2.3‰ at site 1082 and −2.1‰ to −2.7‰ at site 1012. These values compare favorably with our modeled fractionation factors (Table 2), suggesting that, at least at these sites and likely also site 1086, the effect of local exchange reactions on the $\delta^{26}Mg$ value of the pore-fluid is minor. However, the match is not exact; modeled fractionation factors at sites 1082 and 1012 are somewhat larger (e.g., −2.0‰ to –2.7‰) than fractionation factors estimated from measured dolomite samples. This discrepancy could be due to a number of factors including local exchange reactions, the precipitation of multiple Mg-minerals, more closed-system behavior, and/or kinetic isotope effects related to the rate of dolomite precipitation.

5.2. Quantifying the effect of local exchange reactions and multiple Mg-minerals on modeled fractionation factors

At sites where the $\delta^{26}Mg$ value of the pore-fluid stays the same or decreases with depth (1219, 925, and 984) we do not have an independent estimate of either the magnitude of isotopic fractionation associated with mineral precipitation or the gross fluxes of magnesium through the pore-fluid. As a result, at these sites, we cannot exclude the possibility that local exchange reactions and/or multiple Mg-minerals contribute to the observed $\delta^{26}Mg$ profile. However, using isotope mass balance and some simple assumptions about likely $\delta^{26}Mg$ values for dissolving/precipitating minerals, we can at least quantify how these processes would affect our interpretation of modeled fractionation factors. With regard to the precipitation/dissolution of multiple Mg-minerals, consider the simple case where two minerals precipitate. The modeled fractionation factor can be separated into contributions from the two minerals:

$$\varepsilon_{\text{model}}^{26/24} = \varepsilon_1^{26/24} \cdot X_1 + \varepsilon_2^{26/24} \cdot (1 - X_1) \quad (3)$$

where $\varepsilon_{\text{model}}^{26/24}$ is the modeled fractionation factor, $\varepsilon_1^{26/24}$ and $\varepsilon_2^{26/24}$ are the actual fractionation factors associated with the precipitation of mineral 1 and 2, respectively, and X_1 is the fraction of the net magnesium sink that occurs as mineral 1. When $\varepsilon_1^{26/24}$ and $\varepsilon_2^{26/24}$ are very different, as is likely the case for dolomite and Mg-clays (Table 2), minor magnesium sinks (e.g., $(1 - X_1) = 10$–20%) can create large differences between estimated and real fractionation factors. For example, considering $\varepsilon_{\text{model}}^{26/24} = -2.1$‰ and assuming a fractionation associated with Mg-clays ($\varepsilon_2^{26/24}$) of +1.0‰, the real fractionation factor associated with the precipitation of dolomite, $\varepsilon_1^{26/24}$, increases from −2.10‰ to −2.88‰ as the size of the Mg-clay sink increases from 0% to 20% of the total. Thus, minor clay precipitation will lead to underestimates of the fractionation factor associated with dolomite precipitation. Similarly, small amounts of dolomite precipitation will lead to underestimates of the fractionation factor associated with the precipitation of Mg-clays.

If local exchange reactions move magnesium through the pore-fluid at a rate that is significantly greater than the modeled net reaction rates, modeled fractionation factors will reflect the integrated isotopic effects of sources and sinks. In the simple case where one mineral precipitates while another dissolves, $\varepsilon_{\text{model}}^{26/24}$ is a function of the fractionation factor associated with precipitation ($\varepsilon_1^{26/24}$), the $\delta^{26}Mg$ value of the magnesium source ($\delta^{26}Mg_{\text{source}}$), the $\delta^{26}Mg$ value of the pore-fluid ($\delta^{26}Mg_{\text{pore-fluid}}$), the net source/sink term from the model (R_{model}), and the gross sink term (P):

$$\varepsilon_{\text{model}}^{26/24} = 10^3 \cdot \left(\frac{\frac{\delta^{26}Mg_{\text{pore-fluid}}}{10^3} + 1}{\frac{\delta^{26}Mg_{\text{source}}}{10^3} + 1} \cdot \frac{P - R_{\text{model}}}{2P - R_{\text{model}}} + \left(\frac{\varepsilon_1^{26/24}}{10^3} + 1 \right) \cdot \frac{P}{2P - R_{\text{model}}} - 1 \right) \quad (4)$$

Depending on the difference between the isotopic composition of the magnesium source and the pore-fluid, local exchange reactions can lead to large differences between modeled and real magnesium isotope fractionation factors. For example, assuming a modeled fractionation factor ($\varepsilon_{\text{model}}^{26/24}$) of −2.5‰, a $\delta^{26}Mg$ value of the pore-fluid of −0.8‰, and gross precipitation rates that are two times greater than modeled net reaction rates ($P > 2 \cdot R_{\text{model}}$), the real fractionation factor associated with precipitation ($\varepsilon_1^{26/24}$) increases from −2.5‰ to −3.3‰ to −5.6‰ as the $\delta^{26}Mg$ of the local source decreases from +1.7‰ to 0‰ to −4.5‰ (Fig. 6).

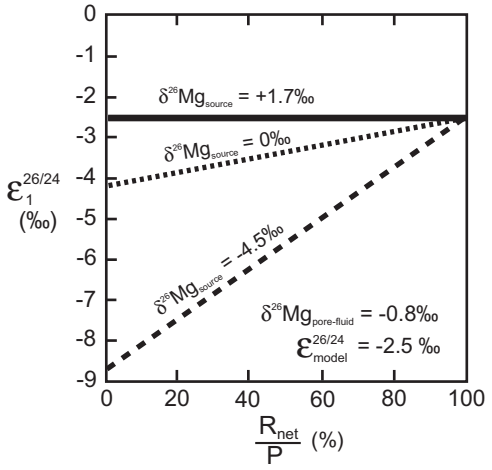

Fig. 6. The effect of local magnesium exchange on our interpretation of modeled net fractionation factors. (R_{model}) is the net reaction rate, P is the rate of gross precipitation, $\varepsilon_1^{26/24}$ is the real fractionation factor for the precipitation of mineral 1, and $\varepsilon_{\text{model}}^{26/24}$ is the modeled net fractionation factor. Lines denote different $\delta^{26}Mg$ values for the local magnesium source. When R_{model}/P is high, modeled fractionation factors will accurately reflect real fractionation factors. When R_{model}/P is low, the $\delta^{26}Mg$ of the local magnesium source becomes important and real fractionation factors may deviate significantly from modeled net fractionation factors.

6. CONCLUSIONS

The widespread observation that magnesium concentrations almost always decrease down core implies Mg-mineral precipitation in the sediment column and/or underlying basalt. The results presented here show that even though concentrations of magnesium in the pore-fluid look similar in many deep-sea sediments, profiles of the δ^{26}Mg values of the pore-fluid may be very different. This observation is best explained by precipitation of different Mg-minerals in the sediment column and/or underlying crust. In half of the studied sites (sites 1082, 1086, and 1012), δ^{26}Mg values increase with depth by up to ~2‰, consistent with the precipitation of a Mg-mineral (dolomite) that is lower in δ^{26}Mg by −2.0‰ to −2.7‰. Measurements of the δ^{26}Mg values of dolomite samples from sites 1082 and 1012 yield fractionation factors for dolomite precipitation that are almost indistinguishable from those determined by the pore-fluid model. The correspondence between modeled fractionation factors and those determined from the dolomite samples indicates that, at least at these sites, local exchange of magnesium between sediment and pore-fluid can be neglected and modeled magnesium isotope fractionation factors can be interpreted as reflecting fractionation factors for dolomite precipitation. At sites 1219, 984, and 925, δ^{26}Mg values of the pore-fluid increase with depth by variable amounts, from <0.2‰ at site 925 to >2‰ at site 984. The increase in δ^{26}Mg values is consistent with a magnesium sink that is isotopically enriched relative to the pore-fluid by between 0‰ and +1.25‰. Although the identity of this magnesium sink is not precisely known, modeled fractionation factors compare favorably to previous work on Mg-clays. More work is needed to constrain the importance of local exchange of magnesium between pore-fluid and sediments at these sites. Our results for all sites are consistent with previous work on magnesium profiles in deep-sea sediment pore-fluids that has focused largely on profile shape and correlative changes in pore-fluid chemistry (e.g., Mg and Ca, alkalinity, K, etc.), mineralogical, and some isotopic (e.g., δ^{18}O of H_2O) observations, to identify the mineral phases involved in magnesium cycling (Gieskes, 1975; Lawrence et al., 1975; Gieskes and Lawrence, 1981; Kelts and McKenzie, 1982). Our work demonstrates the utility of using measurements of magnesium isotopes as a tracer of magnesium sources and sinks in low-temperature aqueous environments and provides new estimates of the magnitude of magnesium isotopic fractionation associated with the slow precipitation of dolomite and Mg-clays in deep-sea sediments.

ACKNOWLEDGMENTS

J.H. received funding from the NSF graduate student fellowship. D.P.S. thanks support from H. Breck and W. Breck. We would like to thank C. Langmuir and S. Jacobsen for use of their analytical facilities. We would like to thank the ODP Program for samples. This manuscript was substantially improved by reviews from F. Richter, M. Fantle, and A. Galy.

REFERENCES

Anderson R. N. and Langseth M. G. (1977) Mechanisms of heat-transfer through the floor of the Indian Ocean. *J. Geophys. Res.* **82**, 3391–3409.

Baker P. A. B. S. J. (1985) Occurrence and formation of dolomite in organic-rich continental-margin sediments. *AAPG Bull. Am. Assoc. Petrol. Geol.* **69**, 1917–1930.

Berner R. A. (1980) *Early Diagenesis*. Princeton University Press, Princeton, NJ.

Boudreau B. P. (1997) *Diagenetic Models and their Implementation: Modelling Transport and Reactions in Aquatic Sediments*. Springer-Verlag, New York.

Carder E. A., Galy A., McKenzie J. A., Vasconcelos C. and Elderfield H. E. (2005) Magnesium isotopes in bacterial dolomites: a novel approach to the dolomite problem. *Geochim. Cosmochim. Acta* **69**, A213.

Carter S. J. R. M. E. and Raymo M. E. J. E. (1999) Sedimentological and mineralogical control of multisensor track data at Sites 981 and 984. In *Proceedings of the Ocean Drilling Program, Scientific Results*. Ocean Drilling Program.

Chang V. T. C., Williams R. J. P., Makishima A., Belshawl N. S. and O'Nions R. K. (2004) Mg and Ca isotope fractionation during $CaCO_3$ biomineralisation. *Biochem. Biophys. Res. Commun.* **323**, 79–85.

Curry W. B., Shackleton N. J. and Richter C. (1995) *Proceedings of the Ocean Drilling Program, Initial Reports* 154.

Fantle M. S. and DePaolo D. J. (2006) Sr isotopes and pore fluid chemistry in carbonate sediment of the Ontong Java Plateau: calcite recrystallization rates and evidence for a rapid rise in seawater Mg over the last 10 million years. *Geochim. Cosmochim. Acta* **70**, 3883–3904.

Fantle M. S. and DePaolo D. J. (2007) Ca isotopes in carbonate sediment and pore fluid from ODP Site 807A: the Ca^{2+}(aq)-calcite equilibrium fractionation factor and calcite recrystallization rates in Pleistocene sediments. *Geochim. Cosmochim. Acta* **71**, 2524–2546.

Galy A., Bar-Matthews M., Halicz L. and O'Nions R. K. (2002) Mg isotopic composition of carbonate: insight from speleothem formation. *Earth Planet. Sci. Lett.* **201**, 105–115.

Galy A., Belshaw N. S., Halicz L. and O'Nions R. K. (2001) High-precision measurement of magnesium isotopes by multiple-collector inductively coupled plasma mass spectrometry. *Int. J. Mass Spectrom.* **208**, 89–98.

Galy A., Yoffe O., Janney P. E., Williams R. W., Cloquet C., Alard O., Halicz L., Wadhwa M., Hutcheon I. D., Ramon E. and Carignan J. (2003) Magnesium isotope heterogeneity of the isotopic standard SRM980 and new reference materials for magnesium-isotope-ratio measurements. *J. Anal. At. Spectrom.* **18**, 1352–1356.

Gieskes J. M. (1975) Chemistry of interstitial waters of marine sediments. *Annu. Rev. Earth Planet. Sci.* **3**, 433–453.

Gieskes J. M. and Lawrence J. R. (1981) Alteration of volcanic matter in deep sea sediments: evidence from the chemical composition of interstitial waters from deep sea drilling cores. *Geochim. Cosmochim. Acta* **45**, 1687–1703.

Hardie L. A. (1996) Secular variation in seawater chemistry: an explanation for the coupled secular variation in the mineralogies of marine limestones and potash evaporites over the past 600 my. *Geology* **24**, 279–283.

Holland H. D. and Zimmerman H. (2000) The dolomite problem revisited. *Int. Geol. Rev.* **42**, 481–490.

Huang F., Glessner J., Ianno A., Lundstrom C. and Zhang Z. F. (2009) Magnesium isotopic composition of igneous rock standards measured by MC-ICP-MS. *Chem. Geol.* **268**, 15–23.

Jansen E., Raymo M. E. and Blum P. (1996) In *Proceedings of the Ocean Drilling Program, Initial Reports*, College Station, TX.

Kelts K. and McKenzie J. A. (1982) Diagenetic dolomite formation in quaternary anoxic diatomaceous muds of DSDP Leg-64, Gulf of California. *Init. Rep. Deep Sea Drilling Proj.* **64**, 553–569.

Lawrence J. R., Gieskes J. M. and Broecker W. S. (1975) Oxygen isotope and cation composition of DSDP pore waters and the alteration of Layer II basalts. *Earth Planet. Sci. Lett.* **27**, 1–10.

Li Y. H. and Gregory S. (1974) Diffusion of ions in seawater and deep-sea sediments. *Geochim. Cosmochim. Acta* **38**, 703–714.

Lyle M., Koizumi I. and Richter C. (1997) In *Proceedings of the Ocean Drilling Program, Initial Reports* 167.

Lyle M., Wilson P. A. and Janecek, T. R. (2002) In *Proceedings of the Ocean Drilling Program, Initial Reports* 199.

Maher K., Steefel C. I., DePaolo D. J. and Viani B. E. (2006) The mineral dissolution rate conundrum: insights from reactive transport modeling of U isotopes and pore fluid chemistry in marine sediments. *Geochim. Cosmochim. Acta* **70**, 337–363.

Mazzullo S. J. (2000) Organogenic dolomitization in peritidal to deep-sea sediments. *J. Sed. Res.* **70**, 10–23.

McDuff R. E. (1981) Major cation gradients in DSDP interstitial waters – the role of diffusive exchange between seawater and upper oceanic-crust. *Geochim. Cosmochim. Acta* **45**, 1705–1713.

McDuff R. E. and Gieskes J. M. (1976) Calcium and magnesium profiles in DSDP interstitial waters: diffusion or reaction? *Earth Planet. Sci. Lett.* **33**, 1–10.

Meister P., Bernasconi S. M., Vasconcelos C. and McKenzie J. A. (2008) Sealevel changes control diagenetic dolomite formation in hemipelagic sediments of the Peru Margin. *Mar. Geol.* **252**, 166–173.

Meister P., McKenzie J. A., Vasconcelos C., Bernasconi S., Frank M., Gutjahr M. and Schrag D. P. (2007) Dolomite formation in the dynamic deep biosphere: results from the Peru Margin. *Sedimentology* **54**, 1007–1031.

Moore T. S., Murray R. W., Kurtz A. C. and Schrag D. P. (2004) Anaerobic methane oxidation and the formation of dolomite. *Earth Planet. Sci. Lett.* **229**, 141–154.

Pearson C. E. (1968) On a differential equation of boundary layer type. *J. Math. Phys.* **47**, 134–154.

Pogge von Strandmann P. A. E. (2008) Precise magnesium isotope measurements in core top planktic and benthic foraminifera. *Geochem. Geophys. Geosyst.* **9**, 13.

Pogge von Strandmann P. A. E., Burton K. W., James R. H., van Calsteren P., Gislason S. R. and Sigfusson B. (2008) The influence of weathering processes on riverine magnesium isotopes in a basaltic terrain. *Earth Planet. Sci. Lett.* **276**, 187–197.

Pufahl P. K. and Wefer G. (2001) Data report: petrographic, cathodoluminescent, and compositional characteristics of organogenic dolomites from the Southwest African margin. In *Proceedings of the Ocean Drilling Program, Scientific Results* 175.

Richter F. M. and DePaolo D. J. (1987) Numerical models for diagenesis and the Neogene Sr isotopic evolution of seawater from DSDP site 590B. *Earth Planet. Sci. Lett.* **83**, 27–38.

Richter F. M. and Depaolo D. J. (1988) Diagenesis and Sr isotopic evolution of seawater using data from DSDP-590B and DSDP-575. *Earth Planet. Sci. Lett.* **90**, 382–394.

Richter F. M., Mendybaev R. A., Christensen J. N., Hutcheon I. D., Williams R. W., Sturchio N. C. and Beloso A. D. (2006) Kinetic isotopic fractionation during diffusion of ionic species in water. *Geochim. Cosmochim. Acta* **70**, 277–289.

Sayles F. L. and Manheim F. T. (1975) Interstitial solutions and diagenesis in deeply buried marine sediments: results from the Deep Sea Drilling Project. *Geochim. Cosmochim. Acta* **39**, 103–127.

Schrag D. P., Depaolo D. J. and Richter F. M. (1992) Oxygen isotope exchange in a 2-layer model of the oceanic-crust. *Earth Planet. Sci. Lett.* **111**, 305–317.

Schrag D. P., Hampt G. and Murray D. W. (1996) Pore fluid constraints on the temperature and oxygen isotopic composition of the glacial ocean. *Science* **272**, 1930–1932.

Teal C. S., Mazzullo S. J. and Bischoff W. D. (2000) Dolomitization of Holocene shallow-marine deposits mediated by sulfate reduction and methanogenesis in normal-salinity seawater, northern Belize. *J. Sed. Res.* **70**, 649–663.

Teng F. Z., Wadhwa M. and Helz R. T. (2007) Investigation of magnesium isotope fractionation during basalt differentiation: implications for a chondritic composition of the terrestrial mantle. *Earth Planet. Sci. Lett.* **261**, 84–92.

Tipper E. T., Galy A. and Bickle M. J. (2006a) Riverine evidence for a fractionated reservoir of Ca and Mg on the continents: implications for the oceanic Ca cycle. *Earth Planet. Sci. Lett.* **247**, 267–279.

Tipper E. T., Galy A., Gaillardet J., Bickle M. J., Elderfield H. and Carder E. A. (2006b) The magnesium isotope budget of the modem ocean: constraints from riverine magnesium isotope ratios. *Earth Planet. Sci. Lett.* **250**, 241–253.

Vasconcelos C. and McKenzie J. A. (1997) Microbial mediation of modern dolomite precipitation and diagenesis under anoxic conditions (Lagoa Vermelha, Rio de Janeiro, Brazil). *J. Sed. Res.* **67**, 378–390.

Von Breymann M. T. and Suess E. (1988) Magnesium in the marine sedimentary environment: Mg—NH_4 ion exchange. *Chem. Geol.* **70**, 359–371.

Vonbreymann M. T., Collier R. and Suess E. (1990) Magnesium adsorption and ion-exchange in marine-sediments – a multi-component model. *Geochim. Cosmochim. Acta* **54**, 3295–3313.

Wefer G., Berger W. H. and Richter C. (1998) In *Proceedings of the Ocean Drilling Program, Initial Reports*, College Station, TX.

Young E. D. and Galy A. (2004) The isotope geochemistry and cosmochemistry of magnesium. *Geochem. Non Trad. Stable Isotopes* **55**, 197–230.

Associate editor: Timothy W. Lyons